WKB APPROACH TO THE PROBLEM OF MHD SHOCK PROPAGATION THROUGH THE HELIOSPHERIC CURRENT SHEET

S. V. URALOVA and A. M. URALOV
Institute of Solar-Terrestrial Physics, Irkutsk 33, 664033 Russia

(Received 7 May, 1993; in revised form 10 February, 1994)

Abstract. The interplanetary shock wave front shape and intensity are calculated numerically by means of the WKB-approach, with nonlinear effects taken into account. The solar flare is modelled as an isotropic point explosion at the solar wind base. The heliospheric current sheet (HCS) is represented by a radially diverging stream with a higher plasma concentration and a lower wind speed. Fast magnetosonic shock wave propagation along the HCS is connected with the effect of regular accumulation of the wave energy in the vicinity of the HCS. In this place the wave intensity is increased, and the corresponding front fragments go ahead to form a shock-wave forerunner as a 'pimple'. The 'primple', in turn, is located inside a quite a large, but less-contrast, 'dimple' in the wave surface. This 'dimple' approximately coincides with the HCS stream contours. If the flare is outside the HCS boundaries, the picture discussed above is conserved, but asymmetry effects arise. Thus the interplanetary shock is stronger when the Earth's observer and the flare are on the same side of the HCS and is weaker in the opposite case.

1. Introduction

The problem of flare-generated shocks propagating through the solar wind has been addressed in a large number of papers. In this regard, the most informative approach is, of course, the method of three-dimensional MHD modelling of heliospheric disturbances (see, for example, Han, Wu, and Dryer, 1988). However, such a modelling is not always possible because of its complexity and labour input. In this paper the problem of propagation of explosive MHD shocks in an inhomogeneous solar wind is solved by a method similar to the method of nonlinear geometric acoustics, or the WKB method (which uses approximate solutions of the same equations under conditions of a smoothly-inhomogeneous medium) (Bazer and Fleischman, 1959; Gubkin, 1961; Korobeinikov, 1967).

In some other form, the WKB method is successfully exploited in many geophysical applications. Conventionally, the method is divided into two procedures. The first procedure does not depend on the second and involves constructing ray trajectories, along which wave front elements propagate. The second procedure involves calculating parameters of the wave as it propagates along the ray. To implement the first procedure has required deriving ray equations in the most general form, and this will be done in Appendix 1. Moreover, the ray equations were supplemented with a term that represents the fact of increasing velocity of the wave front with an increase in shock intensity. Parameters of the wave in this case are calculated on the basis of the known laws of damping of explosive low-intensity MHD shock waves.

Solar Physics **152:** 457–479, 1994.

A preliminary discussion of some results obtained by using the technique suggested here, is contained in papers of Uralova and Uralov (1990) and Eselevich, Uralova, and Uralov (1991). This paper considers in greater detail the problem of interaction of the flare-produced shock wave with the heliospheric current sheet (HCS). The analysis of experimental data does not afford an unambiguous answer to the question: What is the form of the interplanetary shock front in the neighbourhood of the HCS? In other words, it is still unclear where the shock moves faster: near the HCS or far from it? Thus, Watanabe (1989), by analyzing interplanetary scintillation (IPS) data, points to some cases of a strong deceleration of the shock propagating near the HCS. An attempt to give a theoretical interpretation to this result was made by Burton, Siscoe, and Smith (1992). An opposite conclusion that is also based on IPS data, was drawn by Wei and Dryer (1991) by considering a larger sample of data. The work by Dryer *et al.* (1992) who used the method of numerical MHD simulation to examine the interaction of an oblique shock with the HCS, can be regarded as a theoretical substantiation for the last result. In this case, in the vicinity of the HCS there arises a disturbance that travels in the anti-sunward direction faster than the shock that has generated it. The physical nature of this formation, as emphasized by the authors themselves, needs a more detailed analysis.

2. Basic Equations

Ray equations for magnetosonic waves of a linear approximation in an arbitrary orthogonal coordinate system x_i have the form (see Appendix 1):

$$\frac{h_i\,\mathrm{d}x_i}{\mathrm{d}t} = V_i + k\frac{\partial a}{\partial k_i} + a\frac{k_i}{k} \equiv V_i + q_{0i} \equiv q_i\,, \tag{1}$$

$$\frac{h_i\,\mathrm{d}k_i}{\mathrm{d}t} = -\sum_{j=1}^{3}\left[k_j\frac{\partial V_j}{\partial x_i}\right] + \sum_{j=1}^{3}\left[\frac{(V_j k_j)}{h_j}\frac{\partial h_j}{\partial x_i}\right] - k\frac{\partial a}{\partial x_i} + \\ + \frac{a}{k}\sum_{j=1}^{3}\left[\frac{(k_j^2)}{h_j}\frac{\partial h_j}{\partial x_i}\right] - k_i\sum_{j=1}^{3}\left[\frac{\partial h_i}{\partial x_j}\frac{\mathrm{d}x_j}{\mathrm{d}t}\right]\,, \tag{2}$$

$$\frac{\mathrm{d}\omega}{\mathrm{d}t} = \left(\mathrm{k}\frac{\partial \mathbf{V}}{\partial t}\right) + k\frac{\partial a}{\partial t}\,. \tag{3}$$

Here h_i stands for the Lame coefficients; V_i is the velocity component $\mathbf{V} = \mathbf{V}(\mathbf{r},\, t)$ of an undisturbed solar wind; $a = a(\mathbf{r},\, \mathrm{k},\, t)$ is the phase velocity of magnetosonic waves; k_i represents the components of the wave vector k; $k = |\mathrm{k}|$.

The last two terms in (1) represent the group velocity $\mathbf{q}_0$ of a fast ($a = a_+$) and slow ($a = a_-$) magnetosound wave in an immovable medium. Equation (2) gives a variation in wavelength $\lambda = 2\pi/k$ and the orientation in space of the vector

normal $\mathbf{n} = \mathbf{k}/k$ of the small element of the wavefront as it propagates along the ray. The relationship (3) describes a variation in signal duration $T_1 = 2\pi/\omega$ in a nonstationary medium. If the medium is stationary, then $T_1 =$ constant on the entire path of propagation of the linear acoustic wave: $\omega = ak + (\mathbf{k}\cdot\mathbf{V}) =$ constant. This case will be used in our subsequent discussion.

Traditionally, the method of nonlinear geometrical optics presupposes the propagation of each small element of the shock front along its ray constructed on the basis of the linear approximation relationships (1) and (2). In this case the nonlinear evolution of the disturbance itself is studied on the basis of laws of damping of solitary MHD shock waves of low intensity in a smoothly-inhomogeneous medium. For an explosive shock, whose compression phase has the form of a rectangular triangle, such laws may be taken from a paper of Uralov (1982). In this case the relationships of nonlinear geometric acoustics are valid for the jump of the longitudinal gas velocity component in the discontinuity U_{Sh} and the compression phase duration $T_{Sh} = L_{Sh}/q_n$:

$$\begin{aligned} U_{Sh} &= U_1(1 + \tau_1/T_1)^{-1/2}\,, \\ T_{Sh} &= T_1(1 + \tau_1/T_1)^{1/2}\,, \end{aligned} \tag{4}$$

where

$$\tau_1 = \int_{l_*}^{l} \kappa U_1 \,\mathrm{d}l/qq_n\,, \quad (\mathrm{d}l)^2 = \sum_i (h_i\,\mathrm{d}x_i)^2\,,$$

$$q = \Big(\sum_i q_i^2\Big)^{1/2}, \quad q_n = (\mathbf{V}\cdot\mathbf{k})/k + a\,, \tag{5}$$

$$\tfrac{1}{2} \le \kappa = 1 + \partial\,\ln a/\partial\,\ln\rho \le \frac{\gamma+1}{2}\,.$$

Here l is a coordinate counted off along the ray, and l_* is the position of the initial point, at which initial parameters of the selected part of the shock front are determined: $T_{Sh} = T_* = T_1(l_*)$, $U_{Sh} = U_* = U_1(l_*)$. The quantities U_1 and T_1 represent, respectively, the shock intensity and duration obtained in the linear acoustic approximation. In a stationary wind $\mathrm{d}T_1/\mathrm{d}t = 0$, and the quantity U_1 is defined by the expression (see Appendix 2)

$$Sq_n\rho U_1^2(1 + \mu^2)\frac{q_n}{a} = \text{constant}\,, \tag{6}$$

where S is the surface area of the wave front's small element propagating inside the calculated ray tube and $\rho U_1^2(1 + \mu^2)/2$ is the kinetic energy density of a magnetosonic disturbance in a stationary medium.

Equation (1) neglects the fact that in the approximation of nonlinear geometrical acoustics the shock front travels along the normal with a velocity that exceeds the phase velocity by $\kappa U_{Sh}/2$. This follows from conditions on the MHD discontinuity to an accuracy of about ρ'/ρ. Therefore, a correction of Equation (1) for nonlinearity has the form (see also Appendix 3)

$$\frac{h_i\,\mathrm{d}x_i}{\mathrm{d}t} = V_i + k\frac{\partial a}{\partial k_i} + \left(a + \frac{\kappa U_{Sh}}{2}\right)\frac{k_i}{k}\,. \tag{1'}$$

Equations (1'), (2), (4), and (6) serve as the basis for calculating the parameters U_{Sh} and T_{Sh} of the solitary shock wave and the position of its front in a stationary (T_1 = constant) solar wind.

3. The Problem Statement and the Scheme for Numerical Calculation

We are using a spherical-coordinate system, with the Sun lying at its center. In this case, in Equations (1') and (2), one should put $x_1 = r$, $x_2 = \theta$, $x_3 = \varphi$; $h_1 = 1$, $h_2 = r$, $h_3 = r\sin\theta$. The equatorial plane is defined by the condition $\theta = \pi/2$. The model of an undisturbed solar wind is specified analytically and is not intended to be rigorous. In this case for the distances $r' = r/R_\odot \geq 2$, where $R_\odot$ is the solar radius, the following statements are employed. The undisturbed wind is strictly radial, $V_\varphi = V_\theta = 0$. The plasma density of a 'mean' wind is (Yakovlev, Yefimov, and Rubtsov, 1988)

$$\frac{\rho}{m_i} = 1.26 \times 10^7/(r')^2\,V_r' \quad (\mathrm{cm}^{-3})\,, \tag{7}$$

where $V_r' = V_r/10$ km s^{-1} is the radial component of the wind velocity that is specificied separately. The sound velocity is $C(r' \leq 18) = 165$ km s^{-1},

$$C(r' > 18) = 165(18/r')^{2/3} \quad (\mathrm{km\ s}^{-1})\,,$$

which corresponds to lower coronal temperature of 10^6 K with a temperature at the Earth's orbit of 3.6×10^4 K. The radial component of the interplanetary magnetic field $B_r = (r')^{-2}$ G, such that $B_r(r' = 215) = 2.16 \times 10^{-6}$ G. The azimuthal component is defined by the expression

$$B_\varphi = B_{\varphi 0}\frac{(r'-2)}{r'}\,;$$

$$B_{\varphi 0} = B_r\Omega_\odot\frac{r\sin\theta}{V_r} = \frac{0.135\sin\theta}{(r'V_r')} \quad (\mathrm{G})\,, \tag{8}$$

where $B_{\varphi 0}$ corresponds to the familiar supposition about the colinearity of the vectors $\mathbf{B}$ and $\mathbf{V}$ in a coordinate system corotating with the Sun. The correction

factor $(r'-2)/r'$ serves to include this condition at a small distance from the solar surface. Otherwise, the value of B_φ becomes unrealistically large in the region of solar wind formation.

The solar flare is modelled by a point explosion with the coordinates $\mathbf{r}_* = \{r_*, \theta_*, \varphi_*\}$. The initial quantity in this case is the explosion's energy ϵ, expressed in terms of the length parameter

$$\Lambda = \Lambda(\epsilon, \mathbf{k}_*/k_*, \mathbf{r}_*) = \sqrt[3]{\epsilon/\rho_* a_*^2}\,, \tag{9}$$

similar to the length parameter in the theory of a strong explosion in the gas. In this case the product $\rho_* a_*^2$ is proportional to a total (magnetic+gas) pressure in the neighbourhood of the explosion. Here $a_* = a(\mathbf{k}_*/\mathbf{k}_*; \mathbf{r}_*)$ and $\rho_* = \rho(\mathbf{r}_*)$ are the velocities of a fast magnetosonic wave and the plasma density at the explosion point, respectively.

The physical meaning of the quantity Λ lies in the fact that a shock wave, while propagating from the point of explosion in a given direction $\mathbf{k}_*/k_*$, becomes sufficiently weak only when it reaches some reference surface. The location of this surface, with no wind present, roughly accords with the equality $\mathbf{r}_c \approx \mathbf{r}_* + \mathbf{k}_*\Lambda/k_*$. The formation of the explosive disturbance profile is largely completed by this same time, and the profile assumes the form of an explosive wave. These circumstances determine the applicability of the laws of nonlinear damping (Equation (4)) after the wave has passed the reference surface ($t > t_c$). To employ these laws, it is necessary to specify the shock intensity and duration at time $t = t_c$ when the shock intersects this surface ($l = l_*$ in the relationship (5)). The known solution of this question for a point explosion in the gas without a magnetic field (Kestenboim, Roslyakov, and Chudov, 1974), and also considerations based on the dimensional theory permit the initial conditions (as a rather good approximation) for Equations (4) and (5) to be specified as $T_{Sh}(t_c) = T_1 = \Lambda/a_*$, $U_{Sh}(t_c) = U_1(l_*) = a_*$, $\tau_1(t_c) = 0$.

A calculation of the ray pattern starts at time $t = 0$ of departure of the rays from the explosion point. Therefore, initial values of x_i in Equations (1′) and (2) correspond to coordinates of the explosion point $\mathbf{r}_*$. In the interval $0 < t < t_c$ (inside the explosion cavity) the value of $U_{Sh} = a_*$ in Equation (1′). The value of t_c itself, however, is taken to be equal to $\Lambda/(a_* + \kappa U_{Sh}/2)$ as though the explosion occurred in a stationary homogeneous medium. In such a case, Equation (1′) includes the influence of a statinary solar wind upon the shape and location (transport together with the wind) of the explosive cavity. (This influence becomes highly important if the hypothetical point of explosion is transferred to large distances from the solar surface where the wind becomes supersonic (Uralova and Uralov, 1990).

The choice of the initial direction of departure from the explosion point of any one of the rays determines the initial values of k_i specified for Equations (1′) and (2). The latter quantities are readily expressed in terms of the vector $\mathbf{k}_* = k_r \mathbf{e}_r \equiv \mathbf{e}_r$

if a local spherical coordinate system $(1, \theta_0, \varphi_0)$, located at the explosion point, is used. In such a case, a flat fan of equidistant (in angle θ_0) vectors $\mathbf{k}_*$ of unit length $|\mathbf{k}_*| = 1$ corresponds to an equidistant series, for example, of values of θ_0 at a fixed value of φ_0.

A numerical solution of Equations (1′), (2), and (5) is carried out following the Runge–Kutta scheme. The ray tube, inside of which the propagation of a selected part of the wave front of area S occurs, consists of three closely-spaced rays. The value of S is calculated by the Geron formula (Bronshtein and Semendyaev, 1980).

Preliminary calculations have also shown a weak difference of the results obtained both through an accurate calculation of the quantities κ and μ, according to the expressions (5) and (A20) and by using a much simpler replacement $\kappa = 1$ and $\mu = 0$. In what follows we will be using the last variant, which makes the calculation easier.

4. The Heliospheric Current Sheet Influence upon Shock Propagation

The HCS region is modelled by a low-speed and denser solar wind stream. The radial component of a generalized velocity of fast magnetosound ($\approx V_r + a$) in such a stream is lower than that outside the stream. This obviously means that the HCS region exhibits waveguide properties with respect to fast-type disturbances. We have briefly discussed this issue in our earlier paper (Uralova and Uralov, 1990). In this case, special attention should be paid to the fact of radial divergence of this refraction waveguide, which ultimately leads to the effect of regular accumulation of the wave energy in the neighbourhood of the HCS.

In view of the graphic representation of results of calculations on a small computer, we now discuss the simplest variant with the HCS, lying in the equatorial plane. The dependence of the solar wind velocity of angular coordinates is

$$\begin{aligned} V_r &= V_0(r)\left\{1 - \eta\cos^2\left[\frac{\pi(\theta - \pi/2)}{2\Delta\theta_s}\right]\right\}, \quad 0 \le \left|\theta - \frac{\pi}{2}\right| \le \Delta\theta_s, \\ V_r &= V_0(r), \qquad\qquad \left|\theta - \frac{\pi}{2}\right| > \Delta\theta_s, \end{aligned} \tag{10}$$

such that $\partial/\partial\varphi = 0$. The function $V_0(r)$ is the approximation of one of Parker's solutions:

$$V_0(r') = \begin{cases} 1 + 3(r' - 2), & 2 \le r' \le 6, \\ 13 + 1.125(r' - 6), & 6 \le r' \le 30, \\ 40, & r' > 30. \end{cases} \tag{11}$$

The expression (10) represents an axisymmetric, low-speed solar wind stream located inside a sector of half-width $\Delta\theta_s = 10°$. The equatorial plane $\theta = \pi/2$ is a symmetry plane, on which the wind velocity reaches its minimum value equal to

$(1-\eta)V_0(r)$. According to (7), the plasma density here increases $1/(1-\eta)$ times. The value of $\eta = 0.1$ will be used in the calculations to follow. With distance from the equatorial plane, the solar wind velocity increases gradually to reach $V_0(r)$ on the boundary $\theta = \pi/2 \pm \Delta\theta_s$; subsequently, it remains unchanged. On the HCS boundaries the solar wind density and velocity undergo a weak discontinuity.

The solar flare is modelled by a point explosion of energy $\epsilon = 5 \times 10^{30}$ ergs, lying at the distance $r_* = 2\,R_\odot$ from the solar center, $\varphi_* = 0°$. We discuss the situation of a central $\theta_* = 90°$ and lateral explosion $\theta_* = 70°$.

4.1. Consider the first situation when the flare is located in the middle of the HCS. The geometry of the problem in the (r, θ)-plane is shown in Figure 1. The solar wind velocity profile is depicted qualitatively at the right. The HCS boundaries are marked by radial heavy lines. For the sake of convenience, only part of the rays with the initial angles of departure 0–24° southward of the equatorial plane are shown. The northern group of rays can be obtained by a mirror reflection of the southern group of rays with respect to the plane $\theta = 90°$.

We are interested in the nonlinearity effect on the position and shape of the wave front. Therefore, we will not discuss in detail such points as (a) a variation of the time profile of a shock as the carrier ray is reflected from the caustic region, (b) the cross-intersection of shocks of the fronts, typical of phenomena with explosive energy accumulation, and (c) the cross-intersection of ray tubes when their mutual influence is to be taken into account. Of course, all these factors make a correct application of the WKB method difficult (see also Appendix 3). Nevertheless, the results obtained reflect the trends to be expected in numerical MHD modelling of the process of propagation of explosive shock waves along the HCS. In this case the WKB technique results in positions of shock fronts at consecutive times $t_1 - t_5$ (solid heavy lines in Figures 1–3).

The initial, nearly spherical shape of the front of the shock at some distance from the explosion undergoes a particularly marked deformation inside the HCS sector. Initially, a dimple appears on the wave surface ($t = t_1$). As the shock propagates, the dimple becomes ever deeper and wider and leaves the HCS boundaries. However, a pimple ($t = t_2$) develops in the central part of this extensive dimple, with its wave structure becoming increasingly more complex (t_3, t_4, t_5). The formation of the pimple is associated wholly with the intensity redistribution of the shock along its front. The shock attains the highest intensity in the immediate vicinity of the HCS, which – in agreement with Equation (1′) – leads to an advance of corresponding portions of the shock front. The traditional use of the method of nonlinear geometrical acoustics when ray equations (1) and (2) of a linear approximation are used, does not reveal such a pimple. Heavy dots in Figures 1–3 show the position of the front, corresponding to such a calculation when in Equation (1′) the term containing U_{Sh} is omitted. It should be noted that the ray pattern in this case also changes and does not coincide with the depicted one. The HCS waveguide now traps the maximum possible number of rays. With increasing

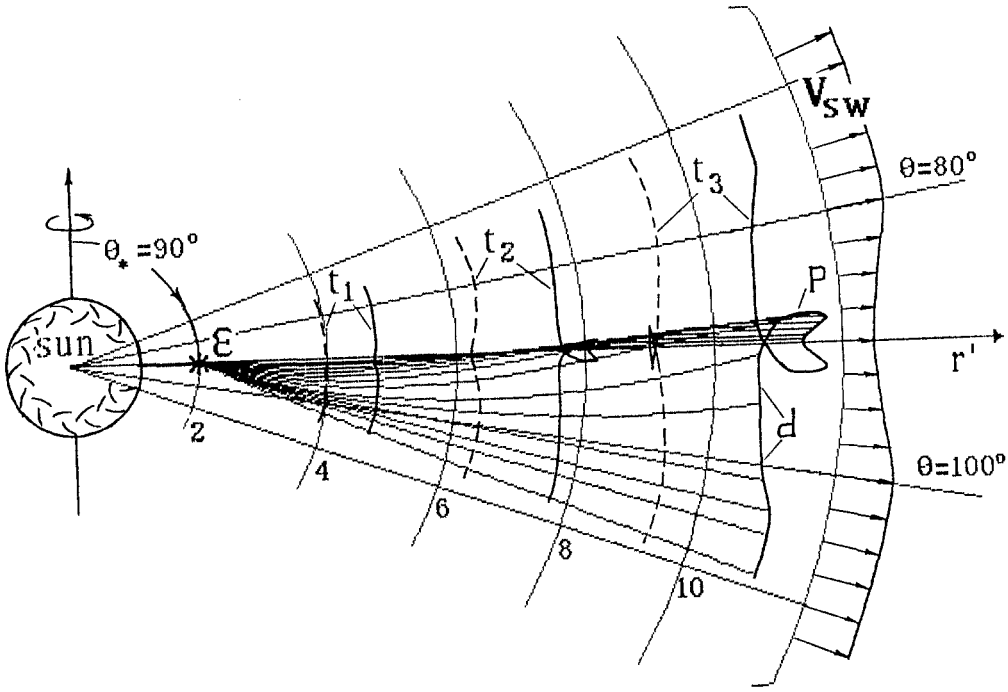

Fig. 1. The problem geometry in the (r, θ)-plane for the case of a central explosion, $\theta_* = 90°$, $r'_* = 2$, $\varphi_* = 0$. To the angle $\theta = 90°$ there corresponds an equatorial current sheet. Inside the sector $\theta = 90° \pm 10°$ the solar wind velocity $v_{S.W.}$ is decreased, and its density is increased. Shown are the trajectories of the rays that originate from the explosion point ϵ in the southward direction. For different times t_1, t_2, and t_3 the position of the shock front from an isotropic explosion of $\epsilon = 5 \times 10^{30}$ ergs is shown, with the nonlinear factor taken (solid heavy line) and not taken into account (heavy dashes) when calculating the ray pattern. The last case actually corresponds to the approximation of linear acoustics when $\epsilon \to 0$. One can see the formation of the shock wave forerunner as a pimple (marked by 'p') as well as the formation of a dimple (marked by 'd').

explosion energy, the waveguide properties of the HCS manifest themselves ever more weakly.

The shock wave forerunner in some range of distances (times $t_2 - t_4$) leads those parts of the shock front which lie outside the HCS sector. At larger distances ($t = t_5$), however, this lead becomes inconspicuous. In the approximation used this result depends weakly on the explosion power ϵ. This is evident from Figure 3, in which the dash-dotted line shows the surface of the shock front from which the hypothetical explosion of $\epsilon = 10^{32}$ erg energy (incidentally, not amenable to the analysis by the WKB method merely because the extent of the compression phase of the explosive wave exceeds, from the very beginning, the transverse size of the θ-inhomogeneity of the calculated ray pattern). This figure also shows clearly the cumulative HCS effect when rays originating from the explosion point are not simply captured by the HCS waveguide (Figures 1 and 2) but concentrate in its central part (seel also Figure 5). The ray channel, following a certain narrowing,

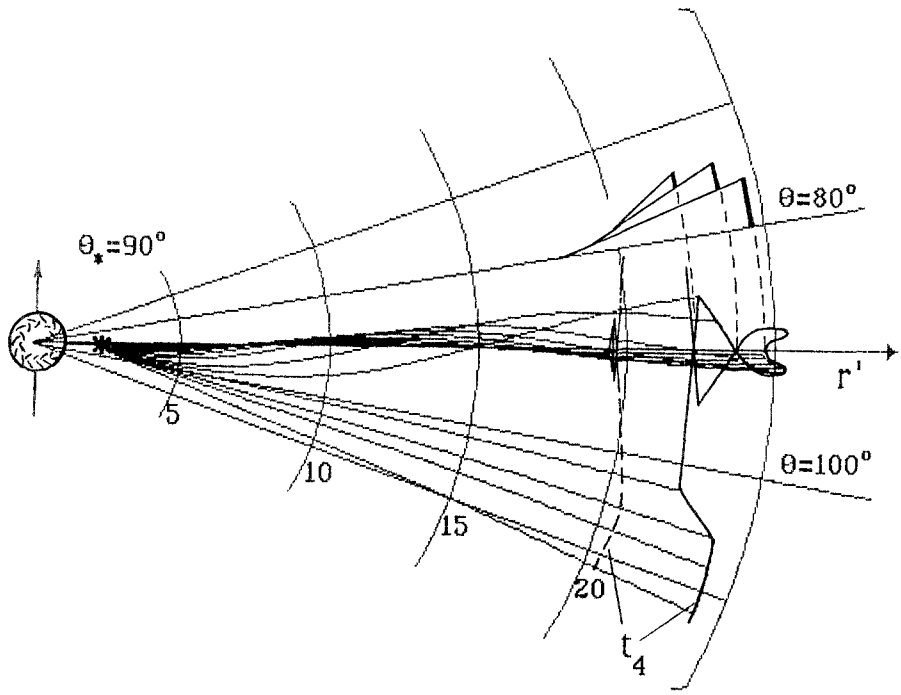

Fig. 2. Same as in Figure 1, but for the subsequent time t_4. The structure of the HCS forerunner becomes more complicated and forms a group of oblique shock waves following each other along the HCS. The equatorial plane is a symmetry plane. At the top, the calculated intensity and extent of the shocks are shown on a relative scale at corresponding (dashed) points of the equatorial plane.

almost does not undergo any expansion in the θ-direction. Suppose now that instead of the complicated wave structure such as shown the ray method, the shock wave forerunner has a simpler form of a solitary wave. This suggests that the wave surface of such a disturbance has a nearly cylindrical divergence (see also Appendix 3). The shock wave forerunner in this case is damped more slowly compared to what is given by our calculation. Therefore, the real lead of the other parts of the shock front by the shock wave forerunner can be more conspicuous.

In addition to other evidence (see Appendix 3), there are the procedure and results of calculations which indicate that the shock wave forerunner should be regarded as a solitary disturbance with a more regular structure than the calculated one. Since the appearance of a forerunner is wholly due to the last term in Equation (1′), its size in the radial direction, in virtue of the relationships (4) and (5), is always smaller than (or, at a large distance from the explosion site, is equal to) the extent of the compression phase of the calculated explosive wave. In this case one must use results of calculations of wave parameters along those ray trajectories which form the leading edge of the shock wave forerunner. An explanation for this is provided by Figure 2, the upper part of which shows, on a relative scale, the calculated intensity U_{Sh} and extent L_{Sh} of the shock waves,

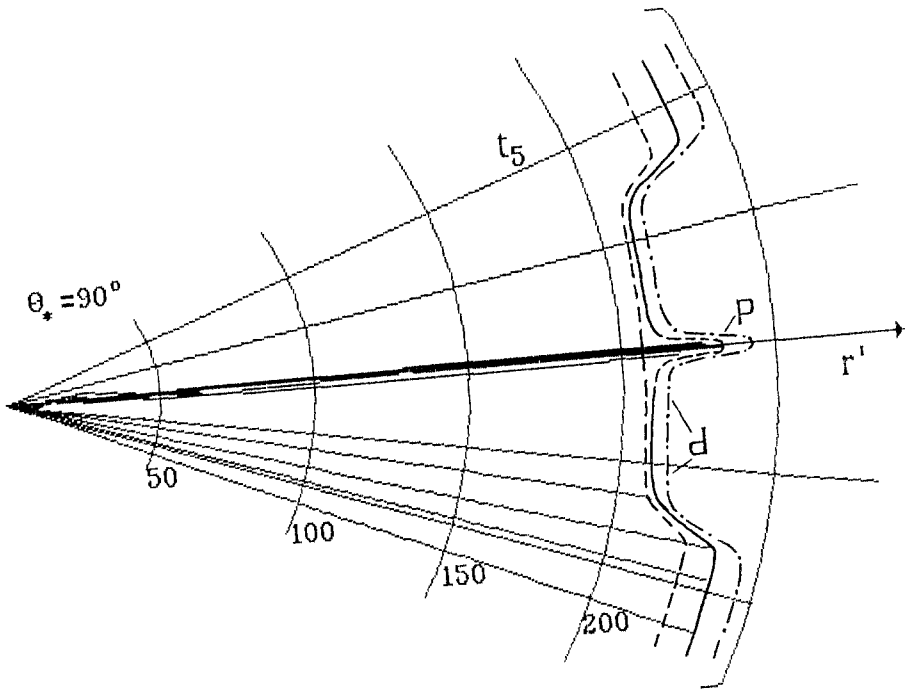

Fig. 3. Same as in Figures 1 and 2, but at a larger distance from the explosion location. Dash-dots indicate the position of the shock front from a hypothetical isotropic explosion $\epsilon = 10^{32}$ ergs; solid heavy line – from explosion $\epsilon = 5 \times 10^{30}$ ergs, heavy dashes – from $\epsilon \to 0$. The complicated structure of the HCS forerunner on this scale is not seen (the region containing it is outlined by dashes).

lying on the equatorial plane at a given time. So large an extent of the 'bow' shock indicated only that the spatial resolution of the shock wave method is insufficient for a correct description of the forerunner structure. On the other hand, a rather obvious conclusion that shocks, following each other, can 'merge' nonlinearly into one, stronger wave, lends support to our inference. With increasing distance from the Sun (after passing still another caustic), the calculated structure of the shock-wave forerunner becomes complicated (there appears still another, new reflected shock). While 'overtaking' and merging with the total disturbance, it 'increases' the disturbance amplitude to an extent such as corresponding to the supposition about the cylindrical divergence of the front of the total shock in the neighbourhood of the HCS. Note also that the 'mean' divergence of the normal cross-section, $\mathcal{S}$, of any individual ray tube exceeds markedly the cylindrical divergence.

In order to provide proof, we make a qualitative assessment of the laws of damping of the shock as it propagates along the HCS. At a large distance from the Sun when the solar wind velocity $V = \text{constant} \gg a$ and the condition $\tau_1 \gg T_1$ is satisfied, from (4), (5), and (6) we get an asymptotic relationship:

$$U_{Sh} \sim U_1/\sqrt{\tau_1} \sim r^{(1-\nu-\delta)/4}\,,$$
$$T_{Sh} \sim \sqrt{\tau_1} \sim r^{(5-\nu-\delta)/4}\,. \tag{12}$$

In this case we put $a \sim r^{-\delta}$, $S \sim r^{\nu-1}$, and take into consideration that $\rho V r^2 =$ constant. The values of $\nu = 3$ and $\nu = 2$, respectively, correspond to spherical and cylindrical divergence of surface S of the shock front. Since $a \sim \sqrt{V_A^2 + c^2}$, where $V_A \sim r^{-1}$ and $c \sim r^{-2/3}$ in our solar wind model, with $c > V_A$, the HCS shock intensity in the case $\nu = 2$ decreases with distance approximately as $U_{Sh} \sim r^{-0.42}$. For the parts of the shock front outside the HCS boundaries $\nu = 3$ and $U_{Sh} \sim r^{-0.66}$. In solar wind models when at large distances from the Sun $V_A > c$, we get $U_{Sh}(\nu = 2) \sim r^{-0.5}$ and $U_{Sh}(\nu = 3) \sim r^{-0.75}$.

Near the explosion site when the shock is very strong and still 'feels' the influence of the explosion point, we have $\epsilon \sim Pr^\nu \sim \rho U_{Sh}^2 r^\nu$, where P is the mean pressure in the explosion cavity, and ρ is the plasma density ahead of the shock front. (Physical processes occurring in the explosion plane, are omitted in our WKB consideration by introducing the notion of a 'check' surface.) The condition $\rho V r^2 =$ constant gives in this case $U_{Sh} \sim \sqrt{\epsilon V(r)}\, r^{(2-\nu)/2}$. If the fact of the HCS cumulative effect is somehow conserved and for a strong explosive shock wave $(2 < \nu < 3)$, then a hypothetical growth of its intensity is possible where the solar wind accelerates (even in the absence of a 'piston'). One must, however, remember the demonstrative character of the scenario just described.

Despite the foregoing discussion, we will, nevertheless, discuss briefly some details of the calculated structure of the shock wave forerunner and possible sequences. As is apparent from Figures 1 and 2, a permanent element of its structure is provided by skew shock waves converging to the equatorial plane (the effect disappears with distance from the Sun). This is an indication of the existence (during some time) of plasma flows that have a small velocity θ-component directed toward the HCS. In the situation of the real HCS, this factor is able to initiate the magnetic reconnection process, accompanying the shock wave. The very fact of the release of the energy stored in the neighbourhood of the neutral current sheet can only increase the shock's kinetic energy. It is also possible that the type II radio source is the consequence of a 'forced' flare process that propagates in the wake of the shock wave. Perhaps, the formation (in some cases) of closed magnetic structures (coronal mass ejections) that move along the HCS, is also associated with this.

4.2. The situation with a side explosion is shown in Figures 4 and 5. The calculated ray pattern clearly demonstrates the fact of wave energy redistribution among inhomogeneous solar wind streams. Disturbances of the fast magnetosonic type leave the region of the 'high-speed' stream to the 'low-speed' stream region (contributing, possibly, to the equalization of their velocities). As the shock wave propagates, the number of rays that have penetrated the waveguide, increases, which was not observed in the case of a central explosion. One may say that there exists a part of

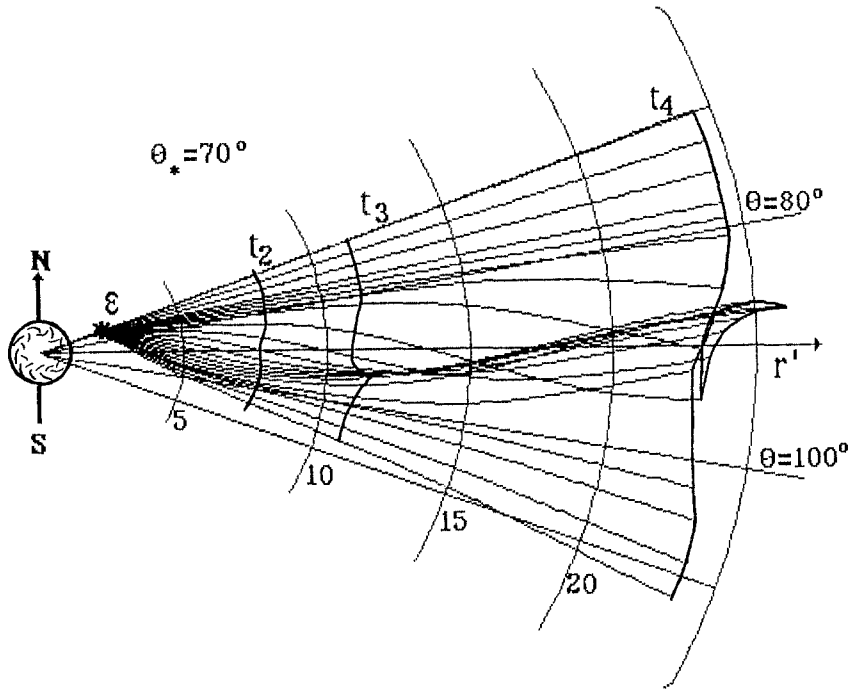

Fig. 4. The problem geometry in the (r, θ)-plane for the case of a side explosion $\epsilon = 5 \times 10^{30}$ ergs with the coordinates of the explosion point $\theta_* = 70°$, $r'_* = 2$, $\varphi_* = 0$. The solar wind model remains the same. Shown are the trajectories of the rays that have in the plane (r, φ) the same angle of departure $\varphi = 0°$ from the explosion point. One can clearly see the 'capture' of a group of rays by the HCS-waveguide. Symbols are the same as for Figures 1–3.

the route, in which the energy of the HCS forerunner increases. However, the total number of rays which are finally captured by the HCS waveguide decreases with increasing latitude of the flare explosion.

In the case of a side explosion, asymmetry effects appear. Thus, the shock strength is higher when the observer and the flare lie on the same side of the HCS (in the northern sector of Figures 4 and 5). A marked attenuation of the shock in the opposite case is due to the existence (in the southern sector of Figures 4 and 5) of an extensive refraction shadow from the HCS waveguide. Outside the refraction shadow region (the southernmost rays in Figures 4 and 5) the shock is only slightly weaker than the one which would be in the absence of the HCS. (This latter is, in part, associated with the fact that in our calculations we used a HCS model with a weakly-expressed θ-inhomogeneity: $\eta = 0.1$ in the expression (10)).

A well-defined 'break' of the large-scale structure of the shock front in Figure 5 is associated with the refraction shadow. Its presence indicates that in a real situation there is a weak 'drift' of the HCS in the southward direction (for the flare that occurred in the northern hemisphere).

The formation process of a shock wave forerunner (as a pimple), as was possible

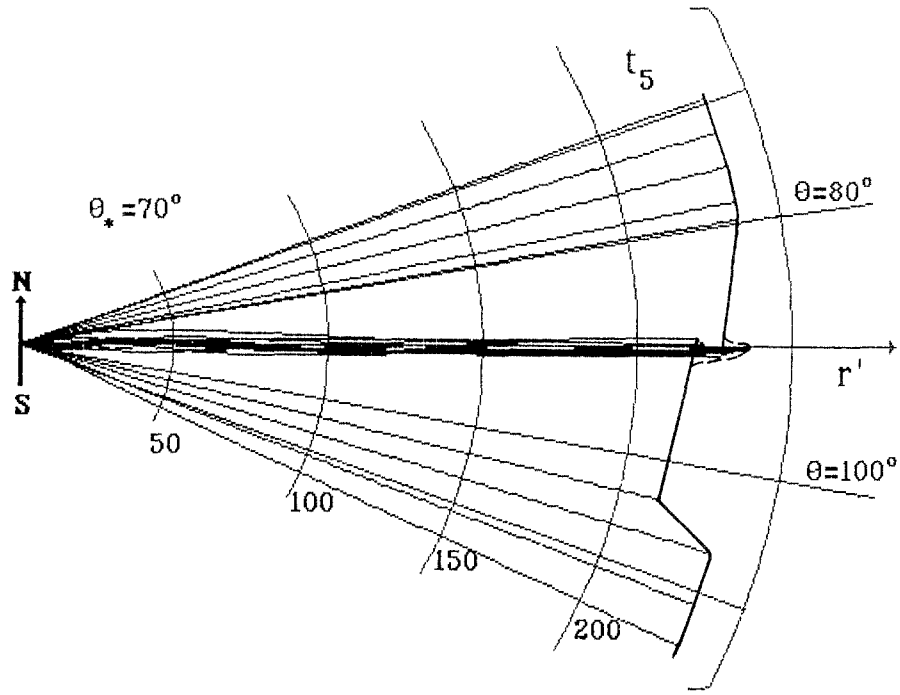

Fig. 5. Same as in Figure 4, but at larger distance from the explosion site. One can clearly see the cumulative effect of a radially-diverging refraction HCS waveguide. The shock is stronger whenever the observer and the flare are on the same side of the HCS and is weaker otherwise.

to study in our numerical simulation, perhaps sheds some light on the nature of the fast disturbance detected by Dryer *et al.* (1992) in a numerical MHD simulation of the shock–HCS interaction process. It should be conjectured that an experimental confirmation of the above distortion of the form of the shock front in the neighbourhood of the HCS is most probable for interplanetary shock waves of moderate intensity (see Appendix 3). In turn, a weakly-expressed HCS does also not give rise to new effects; when $\eta \to 0$ in (10), there is a 'smoothing-out' of the 'dimple–pimple' inhomogeneity of the shock front until its total disappearance.

4.3. So far we have discussed the features of a weak interplanetary shock wave in coordinates (r, θ). As far as the wave surface behaviour in the (r, φ)-plane is concerned, however, we will limit ourselves only to one remark. As the shock propagates, the shock front slowly turns westward. In this case the westward deviation of the central ray that has left the explosion point in the radial direction at the Earth's orbit is $\Delta\varphi = 11°$ for our model. This effect is caused by the asymmetry of the group Fridrichs polar curve for a fast magnetosonic wave when the propagation across the magnetic field is faster than along the field. The turning

of the shock front is observable when the shock wave becomes sufficiently weak. The sign of the turning in this case is opposite to the sign of the interplanetary magnetic field spiral.

Appendix 1. The Ray Equations

Constructing the ray pattern is the first stage of the entire computational scheme. Since at each point of the medium there are two distinct directions, one along the solar wind velocity $\mathbf{V}$, and the other along the magnetic field vector $\mathbf{B}$, the medium is twice anisotropic. The medium is also inhomogeneous because all its parameters $\mathbf{V}$, $\mathbf{B}$, density ρ, and gas pressure p vary from point to point. Not the least of the factors is the question of choosing the coordinate system. The point here is that if there are ray equations in Cartesian coordinates, then even in the simplest cases ($\mathbf{V} = \mathbf{B} = 0$) converting to curvilinear coordinates involves unwieldy calculations (Kravtsov and Orlov, 1980). It should also be noted that the frequently-used vector representation of canonical equations is valid only in Cartesian coordinates. In any other coordinates, only Hamiltonian equations of characteristics hold, which are invariant with respect to choosing a particular coordinate system.

Papers on this issue (Weinberg, 1962; Blokhintsev, 1981; Berstein, 1971) contain either simplifying assumptions (for example, $\mathbf{V} = 0$, or $\mathbf{B} = 0$, or $p = 0$) or involve determining only the weak discontinuity surface (Bazer and Fleishman, 1959), thereby neglecting an important parameter, such as the wavelength. Moreover, the form of representation of the terminal expressions often is simply not convenient. Taking all of these factors into account dictated the need to derive ray equations for magnetosonic waves in the most general form.

The starting system is the system of equations of an ideal single-fluid magnetic gas dynamics written as

$$\frac{\partial \rho}{\partial t} + \rho \operatorname{div} \mathbf{V} + \mathbf{V} \cdot \operatorname{grad} \rho = 0 ,$$

$$\frac{\partial \mathbf{V}}{\partial t} + [\operatorname{rot} \mathbf{V} \times \mathbf{V}] + \frac{1}{2} \operatorname{grad} V^2 = -\frac{1}{\rho} \operatorname{grad} p + \frac{1}{4\pi\rho} [\operatorname{rot} \mathbf{B} \times \mathbf{B}] + \mathbf{g} ,$$

$$\frac{\partial S}{\partial t} + (\mathbf{V} \cdot \operatorname{grad} S) = 0 , \tag{A1}$$

$$\frac{\partial \mathbf{B}}{\partial t} = \operatorname{rot} [\mathbf{V} \times \mathbf{B}] ,$$

$$\operatorname{div} \mathbf{B} = 0 ,$$

$$p(\rho, S) = \rho^{\gamma} \frac{p_0}{\rho_0^{\gamma}} \exp[(S - S_0)/c_V] .$$

Here $\mathbf{V}$ and $\mathbf{B}$ are the plasma velocity and the magnetic field in a fixed coordinate system, respectively; ρ and p are the gas density and pressure, respectively; S is the entropy of unit mass; $\gamma = c_p/c_V = \frac{5}{3}$ is the adiabatic exponent and c_V (c_p) is the heat capacity of unit mass at constant volume (pressure). On redenoting by the quantities ρ, p, S, $\mathbf{V}$, and $\mathbf{B}$ the undisturbed solar wind parameters and by ρ', p', S', $\mathbf{V}'$, and $\mathbf{B}'$ their small disturbances, the initial system can be linearized in the usual way (so that $\rho \to \rho + \rho'$, etc.). However, in view of the WKB approximation used, we are seeking a solution in the form

$$(p',\ \rho',\ S',\ \mathbf{V}',\ \mathbf{V}') = ((p'_0,\ \rho'_0,\ S'_0,\ \mathbf{V}'_0,\ \mathbf{V}'_0)\exp(i\psi)\ . \tag{A2}$$

The function ψ that is called the eikonal, is a large value and varies by 2π at the distance of the wavelength λ. Disturbance amplitudes (zero indices) are slowly varying functions of coordinates and, perhaps, of time. On substituting (A2) into (A1) with the use of vector analysis functions, we get

$$\begin{aligned}
&iQ\rho'_0 + i\rho(\mathbf{V}'_0 \cdot \operatorname{grad}\psi) = d_1\ ,\\
&iQ\mathbf{V}'_0 + i\frac{p'_0}{\rho}\operatorname{grad}\psi + \frac{i}{4\pi\rho}(\mathbf{B}\cdot\mathbf{B}'_0)\operatorname{grad}\psi - \frac{i}{4\pi\rho}\mathbf{B}'_0(\mathbf{B}\cdot\operatorname{grad}\psi) = \mathbf{d}_2\ ,\\
&iQS'_0 = d_3\ ,\\
&iQ\mathbf{B}'_0 - i\mathbf{V}'_0(\operatorname{grad}\psi\cdot\mathbf{B}) + i\mathbf{B}(\operatorname{grad}\psi\cdot\mathbf{V}'_0) = \mathbf{d}_4\ ,\\
&i(\operatorname{grad}\psi\cdot\mathbf{B}'_0) = d_5\ ,\\
&p'_0 = \left(\frac{\partial p}{\partial\rho}\right)_S\rho'_0 + \left(\frac{\partial p}{\partial S}\right)_\rho S'_0 = c^2\rho'_0 + \left(\frac{p}{c_V}\right)S'_0\ ,\\
&Q \equiv \partial\psi/\partial t + (\mathbf{V}\cdot\operatorname{grad}\psi)\ .
\end{aligned} \tag{A3}$$

All terms on the left-hand sides of the equations contain an eikonal. The quantities d_i, in turn, consist of terms that do not contain an eikonal and hence are small. In this case:

$$\begin{aligned}
d_1 &= -\frac{\partial\rho'_0}{\partial t} - (\mathbf{V}'_0\operatorname{grad}\rho) - (\mathbf{V}\cdot\operatorname{grad}\rho'_0) - \rho\operatorname{div}\mathbf{V}'_0 - \rho'_0\operatorname{div}\mathbf{V}\ ,\\
\mathbf{d}_2 &= -\frac{\partial\mathbf{V}'_0}{\partial t} + [\mathbf{V}'_0\times\operatorname{rot}\mathbf{V}] + [\mathbf{V}\times\operatorname{rot}\mathbf{V}'_0] - \operatorname{grad}(\mathbf{V}\cdot\mathbf{V}'_0) -\\
&\quad -\frac{1}{\rho}\operatorname{grad}p'_0 + \frac{\rho'_0}{\rho^2}\operatorname{grad}p + \frac{1}{4\pi\rho}[\operatorname{rot}\mathbf{B}\times\mathbf{B}'_0] +\\
&\quad +\frac{1}{4\pi\rho}[\operatorname{rot}\mathbf{B}'_0\times\mathbf{B}] - \frac{\rho'_0}{4\pi\rho^2}[\operatorname{rot}\mathbf{B}\times\mathbf{B}]\ ,
\end{aligned} \tag{A4}$$

$$d_3 = -\frac{\partial S_0'}{\partial t} - (\mathbf{V} \cdot \operatorname{grad} S_0') - (\mathbf{V}_0' \cdot \operatorname{grad} S) ,$$

$$\mathbf{d}_4 = -\frac{\partial \mathbf{B}_0'}{\partial t} + \operatorname{rot}[\mathbf{V}_0' \times \mathbf{B}] + \operatorname{rot}[\mathbf{V} \times \mathbf{B}_0'] ,$$

$$d_5 = -\operatorname{div} \mathbf{B}_0' = 0 .$$

That all quantities d_i go to zero, corresponds to the formation of (A3) of a system of zeroth approximation equations. Equations of this approximation give a linear relationship of the quantities in the short wave of a small amplitude, and also they form the basis for deriving ray equations. Waves of this approximation are iso-entropic ones $S' = 0$ and satisfy the condition $(\operatorname{grad}\psi \cdot \mathbf{B}_0') = 0$. In this case from (A3) one immediately gets $(d_i = 0)$

$$p_0' = c^2 \rho (\mathbf{V}_0' \cdot \operatorname{grad}\psi)/Q . \tag{A5}$$

In the case of magnetosonic waves $p_0' \neq 0$. Then, by mutiplying the second equation in (A3) scaled by $\operatorname{grad}\psi$, using (A5) we find

$$-\frac{Q^2}{c^2\rho} p_0' + \frac{(\operatorname{grad}\psi)^2}{\rho} \left[p_0' + \frac{(\mathbf{B} \cdot \mathbf{B}_0')}{4\pi} \right] = 0 . \tag{A6}$$

In the approximation used, the expression between square brackets is $\rho_0' a^2 = p_0' a^2/c^2$ because for simple magnetosonic waves there exists an accurate expression (Kulikovsky and Lyubimov, 1962)

$$a^2 = \frac{\mathrm{d}}{\mathrm{d}\rho} \left(\frac{B_\tau^2}{8\pi} + p \right) .$$

Here $a = a_{(+,-)}$ are the phase velocities of propagation of (fast, slow) magnetosonic waves of a small amplitude in a homogeneous immovable medium. B_τ is the tangential component of the total magnetic field, and p is the gas pressure in the wave. Hence, $\mathrm{d}B_\tau^2 = 2B_\tau B' = 2(\mathbf{B} \cdot \mathbf{B}')$ because $\mathrm{d}B_n = 0$. In turn, $\mathrm{d}p \approx p'$ and $\mathrm{d}\rho \approx \rho'$. Now, instead of (A6), we get

$$Q^2 - a^2 (\operatorname{grad}\psi)^2 = 0 ,$$

or

$$(Q - a\,|\operatorname{grad}\psi|)\,(Q + a\,|\operatorname{grad}\psi|) = 0 . \tag{A7}$$

These expressions have an obvious meaning. The WKB approximation assumes a wave nondistinguishable from a plane wave in a small range of space and time, such that $\psi = -\omega t + (\mathbf{k} \cdot \mathbf{r})$, where ω is the circular frequency, and $\mathbf{k}$ is a wave

vector. From this we have $\partial\psi/\partial t = -\omega$ and $\operatorname{grad}\psi = \mathbf{k}$. When each of the brackets in Equation (A7) goes to zero, this is represented by the dispersion of magnetosonic waves that propagate in a positive or opposite direction. For the sake of simplicity, we will limit ourselves to a wave running in the positive direction: this corresponds to the second bracket in (A7) going to zero. Thus, we write the eikonal equation for magnetosonic waves:

$$\frac{\partial\psi}{\partial t} + (\mathbf{V}\cdot\operatorname{grad}\psi) + a\,|\operatorname{grad}\psi| \equiv F = 0\,. \tag{A8}$$

The phase velocity of magnetosonic waves is given by a familiar expression (Kulikovsky and Lyubimov, 1962):

$$a_{+,-} = \tfrac{1}{2}\{\sqrt{c^2 + V_A^2 + 2c(\mathbf{V}_A\mathbf{k})/k} \pm \sqrt{c^2 + V_A^2 - 2c(\mathbf{V}_A\mathbf{k})/k}\}\,,$$

where

$$\mathbf{V}_A = \mathbf{B}/\sqrt{4\pi\rho}\,, \quad k = |\mathbf{k}|\,.$$

Assuming in (A5) $(\mathbf{V}_0'\cdot\operatorname{grad}\psi) = 0$, we save out transverse Alfvén waves, for which $(\mathbf{k}\mathbf{B}_0') = (\mathbf{k}\mathbf{V}_0') = (\mathbf{B}\cdot\mathbf{B}_0') = (\mathbf{B}\mathbf{V}_0') = 0$, unlike longitudinal magnetosonic waves. The eikonal equation for Alfvén waves in this case readily follows from (A3):

$$\frac{\partial\psi}{\partial t} + (\mathbf{V}\cdot\operatorname{grad}\psi) + (\mathbf{V}_A\cdot\operatorname{grad}\psi) = 0\,. \tag{A9}$$

We now derive the ray equations of magnetosonic waves in an arbitrary orthogonal curvilinear coordinate system. The eikonal equation for this case must be rewritten as

$$F(\mathbf{P},\,\mathbf{r},\,P_t,\,t) = \sum_{i-3}^{3}\frac{V_iP_i}{h_i} + P_t + a\left[\sum_{i=1}^{3}\frac{P_i^2}{h_i^2}\right]^{1/2} = 0\,, \tag{A10}$$

$$\mathbf{V} = \mathbf{V}(\mathbf{r},\,t)\,; \quad a = a(\mathbf{r},\,\mathbf{P},\,t); \quad \mathbf{P} = \{P_1,\,P_2,\,P_3\}; \quad \mathbf{r} = \{x_1,\,x_2,\,x_3\}\,.$$

Here we have introduced the designations

$$\frac{\partial\psi}{\partial x_i} = P_i\,, \quad \frac{\partial\psi}{\partial t} = P_t\,,$$

taking into consideration that

$$\operatorname{grad}\psi = \sum_{i=1}^{3}\frac{1}{h_i}\frac{\partial\psi}{\partial x_i}\mathbf{e}_i\,,$$

where

$$h_i = \sqrt{g_{ii}} = h_i(x_1, x_2, x_3)$$

are the Lamé coefficients of the curvilinear coordinate system $\{x_1, x_2, x_3\}$. $\mathbf{e}_i$ stands for local base vectors.

The solution of Equation (A10) is the function $\psi(\mathbf{r}, t)$. In turn, (A10) reduces to the following system of ordinary differential (characteristic) equations (Korn and Korn, 1968):

$$\begin{aligned} \frac{\mathrm{d}x_i}{\mathrm{d}\tau} &= \frac{\partial F}{\partial P_i}, \quad \frac{\mathrm{d}\psi}{\mathrm{d}\tau} = \sum_i P_i \frac{\partial F}{\partial P_i}, \\ \frac{\mathrm{d}P_i}{\mathrm{d}\tau} &= -\frac{\partial F}{\partial x_i} - P_i \frac{\partial F}{\partial \psi}, \end{aligned} \tag{A11}$$

where τ is a certain parameter. Assuming formally $P_t = P_4$, $t = x_4$ from (A10) and (A11) we find

$$\frac{\mathrm{d}t}{\mathrm{d}\tau} = 1, \qquad \frac{\partial F}{\partial \psi} = 0, \tag{A12}$$

$$\frac{\mathrm{d}x_i}{\mathrm{d}\tau} = \frac{V_i}{h_i} + |\mathrm{grad}\,\psi| \frac{\partial a}{\partial P_i} + a \frac{P_i}{|\mathrm{grad}\,\psi|\, h_i^2}, \tag{A13}$$

$$\frac{\mathrm{d}\psi}{\partial \tau} = \sum_{i=1}^{3} P_i \frac{\mathrm{d}x_i}{\mathrm{d}\tau} + P_t, \tag{A14}$$

$$\begin{aligned} \frac{\mathrm{d}P_i}{\mathrm{d}\tau} = -\Bigg\{ &\sum_{j=1}^{3} \frac{P_j}{h_j} \frac{\partial V_j}{\partial x_i} - \sum_{j=1}^{3} \frac{1}{h_j^2} \frac{\partial h_j}{\partial x_i} (V_j P_j) + \\ &+ |\mathrm{grad}\,\psi| \frac{\partial a}{\partial x_i} - \frac{a}{|\mathrm{grad}\,\psi|} \sum_{j=1}^{3} \frac{P_j^2}{h_j^3} \frac{\partial h_j}{\partial x_i} \Bigg\} - P_i \frac{\partial F}{\partial \psi}, \end{aligned} \tag{A15}$$

$$\frac{\mathrm{d}P_t}{\mathrm{d}\tau} = -\left\{ \left(\frac{\partial \mathbf{V}}{\partial t} \mathrm{grad}\,\psi \right) + \frac{\partial a}{\partial t} |\mathrm{grad}\,\psi| \right\}. \tag{A16}$$

The first equation means $\tau = t$. Substituting (A13) into (A14) with the use of (A10) yields $\mathrm{d}\psi/\mathrm{d}t = 0$. This means that the equations 'watch' the constant phase velocity surface. Since these are differential equations, trajectories and the orientation in space of only a small part of this surface are traceable. In the remaining equations, instead of the variables P_i and P_t, we use the variables $\mathbf{k}$ and ω. Putting, as usual,

$$P_t = -\omega\,, \qquad \mathbf{k} = \operatorname{grad}\psi = \sum_{i=1}^{3} \frac{P_i}{h_i}\mathbf{e}_i\,, \tag{A17}$$

we find $P_i = P_i(k_i;\, x_1,\, x_2,\, x_3) = h_i k_i$.

We need to express the derivatives $\mathrm{d}P_i/\mathrm{d}t$ and $\partial a/\partial P_i$ in terms of $\mathrm{d}k_i/\mathrm{d}t$ and $\partial a/\partial k_i$. By expressing the total differential $\mathrm{d}P_i = d(h_i k_i)$ in terms of $\mathrm{d}x_j$, $\mathrm{d}k_i$, we obtain

$$\frac{\mathrm{d}P_i}{\mathrm{d}t} = k_i \sum_{j=1}^{3} \frac{\partial h_i}{\partial x_j}\frac{\mathrm{d}x_j}{\mathrm{d}t} + h_i \frac{\mathrm{d}k_i}{\mathrm{d}t}\,, \quad \frac{\partial}{\partial P_i} = \frac{1}{h_i}\frac{\partial}{\partial k_i}\,. \tag{A18}$$

Substituting (A18) into (A13), (A15) , (A16) gives the desired ray equations (1), (2), (3) in an arbitrary orthogonal coordinate system (Section 2).

As has been pointed out, Equations (1) and (2) allow for a vector representation in Cartesian (and only in Cartesian) $h_i = 1$ coordinates. The inverse transition to curvilinear coordinates using vector analysis formulae is not correct, however.

Appendix 2. The Law of Variation of the Linear Wave Amplitude

Such a law can in principle be obtained from the system of first-approximation equations. These equations follow from (A3) if solutions of the zeroth-approximation are substituted into the expression d_i (A4). However, owing to the obvious unwieldy character of the general derivation, we will take a different line.

We avail ourselves of the known fact that in the first approximation the energy flux in the ray tube is conserved. In an immovable medium (or, equivalently, in a frame of reference that moves together with the wind) the mean density $\Delta\epsilon_0$ of excess energy in the wave is composed of the potential and kinetic energy. In a linear magnetosound wave (in the case of an Alfvén wave, even without a limitation on its amplitude) the values of $\Delta\epsilon_0$ are of second order of magnitude equal to the double density of mean kinetic energy, $\Delta\epsilon_0 = \rho\overline{(u^2 + v^2)}$, where u and v are, respectively, the normal (along wave vector) and tangential plasma velocity components in the wave. The wave energy flux in the ray tube with a normal cross-section $\mathcal{S}$ in this case is simply $F_0 = \mathcal{S}\Delta\epsilon_0 q_0$, where q_0 is the group velocity of the wave in an immovable medium. If, however, the medium travels in the direction of propagation of the wave, then the velocity of wave energy transfer with respect to the immovable observer will also increase: $F_1 = \mathcal{S}\Delta\epsilon q$. In turn, $\Delta\epsilon_0 = \Delta E/\lambda_0$, where ΔE is the total wave energy contained in a volume of unit cross-section, whose length equals the wavelength $\lambda_0 = aT_1$. The transition from one system of reference to another must not change the value of ΔE. However, the wavelength, λ, in this case varies because its duration $T_1 = 2\pi/\omega$ defined by Equation (3), remains the same with such a procedure. Therefore, $\lambda = q_n T_1$ and, accordingly, the real value of mean wave energy density will be

$$\Delta\epsilon = \rho\overline{(u^2 + v^2)} = \Delta E/\lambda = \Delta\epsilon_0\lambda_0/\lambda\,.$$

Conservation of the wave energy flux in the ray tube is now written

$$F_1 = \mathcal{S} q \rho (u^2 + v^2) \frac{q_n}{a} = \text{constant} . \tag{A19}$$

It should be noted that a more rigorous derivation of such a WKB relationship is contained in a recent paper by Barnes (1992).

From the relationships of magnetosonic waves of small amplitudes (Kulikovsky and Lyubimov, 1962) it also follows that

$$\frac{v^2}{u^2} = \mu^2 = \left(1 - \frac{c^2}{a^2}\right) \operatorname{cotg}^2 \beta , \tag{A20}$$

where β is the acute angle between the vectors $\mathbf{B}$ and $\mathbf{k}$:

$$\operatorname{cotg} \beta = \frac{B_n}{B_\tau} = \frac{(\mathbf{B} \cdot \mathbf{n})}{\sqrt{\mathbf{B}^2 - (\mathbf{B} \cdot \mathbf{n})^2}} .$$

A special case is the case of $\beta = 0$ and $a_+ = V_A$ when the linear approximation is insufficient: $\mu^2 \approx 2(V_A^2 - c^2)/uV_A$.

In our numerical calculations, we are using the quantity S, the area of the part of the wave front in the ray tube which in the general case is by no means equal to the area of its normal cross-section. These quantities are related by the relationship $S = \mathcal{S} q / q_n$. In view of the above-said, as well as using the fact that the form of a disturbance in the linear WKB-approximation does not change, we rewrite (A19) as (6) in Section 2.

Appendix 3. Generalization to the Case of Strong Shock Waves

Let $f = f(\mathbf{r}, t)$ be the equation of a shock front surface. To the differential equation of the surface there corresponds the equality $\mathrm{d}f = 0$, from which for the group displacement velocity of a small element of the shock front we get

$$\frac{\mathrm{d}\mathbf{r}}{\mathrm{d}t} = -\frac{\partial f / \partial t)}{(\partial f / \partial \mathbf{r})} = \mathbf{q} = \mathbf{q}_0 + \mathbf{V} . \tag{A21}$$

The vector $(\partial f / \partial \mathbf{r})$ coincides in direction with the wave normal vector $\mathbf{n}(= \mathbf{k}/k)$. In the case of linear magnetosonic and Alfvén waves, Equation (A21) immediately gives equations that coincide with the corresponding eikonal equations (A8) and (A9), with the only difference that instead of the eikonal ψ we now have the function f. The formal replacement $\partial f / \partial \mathbf{r} = \mathbf{k}/k$, $\partial f / \partial t = -\omega$; makes the following procedure for deriving ray equations identical.

A.3.1. WEAK SHOCK CASE

In this case $\mathbf{q} = \mathbf{V} + \mathbf{q}_0 + \mathbf{n}(\kappa U_{Sh}/2)$. The corresponding eikonal equation in this case coincides with Equation (8) when the phase velocity a is substituted by $a' = a + \kappa U_{Sh}/2$. Therefore, in Equations (1), (2), and (3) it is also necessary to make the same replacement. In the new 'ray' equations there now appear additional terms $(\partial/\partial k_i, \partial/\partial x_i)\kappa U_{Sh}$ which are very difficult to calculate. Expressions such as $\partial(\kappa U_{Sh})/\partial k_i$ may be omitted, in view of their small magnitude. Then, instead of (1) we get (1′) which we did use.

The first and third terms on the right-hand side of Equation (2) are the main factor that determine the effect of ray refraction in our model. In the linear approximation the term of the form $\partial(V + a)/\partial\theta$ is responsible for the manifestation of waveguide properties of the HCS region, which ultimately leads to an enhancement (on average) of the shock in the immediate neighbourhood of the HCS. In this case, however, the role of the 'nonlinear' refraction that acts in the backward direction increases. This effect is caused by the appearance in (2) of an additional term $\sim\partial(\kappa U_{Sh})/\partial\theta$. While the usual (linear) refraction imparts focusing properties to the heliospheric waveguide, the 'nonlinear' refraction contributes to an expansion of the calculated wave pattern in the θ-direction, with the expansin increasing with increasing nonlinearity. A hypothetical limit is the acquisition by the front of a quasi-stationary form when $\partial(V + a + \kappa U_{Sh}/2)/\partial\theta \approx 0$. It is clear that as long as the nonlinearity is small, the factor of linear refraction is dominant, and we are justified in using Equation (2) in our calculations.

It should be noted that the nonlinear refraction effect reflects a tendency of the shock intensity to equalize along its front (as well as a tendency of wave surface unevennesses to smooth) as in the case of diffraction effects. Taking these latter into account is also beyond the scope of the WKB method.

A.3.2. STRONG SHOCK CASE

The shock is assumed to be so strong that the magnetic field influence is neglected. In this case $\mathbf{q} = \mathbf{V} + \mathbf{D}$, where $\mathbf{D} = \mathbf{n}D_n + \boldsymbol{\tau}D_\tau$ is the group velocity of a strong-gas dynamic shock wave in an immovable medium. $D_n = [(\gamma+1)P/2\rho]^{1/2}$, where P ($\gg B^2/8\pi$) is the gas pressure behind the front, and ρ is the density ahead of the front. A corresponding 'eikonal' equation coincides with (A8), provided there is the replacement $a \to D_n$. The same replacement should be done in ray equations (1)–(3). It should be kept in mind, however, that in this case the notion of the wavelength $\lambda = 2\pi/k$ and its duration $2\pi/\omega$ has a formal meaning. Equation (2) should be regarded in this case as the equation of wave normals.

The subsequent solution of the problem of determining the surface of the front depends on the method of specifying the quantity D_n. In this connection, we wish to note a recent paper by Burton, Siscoe, and Smith (1992), who discuss the propagation of a strong shock wave in a symmetric wind. In this case the equatorial current sheet is modelled on the (r, θ)-plane by a sector, inside which

($|\theta - \pi/2| < \Delta\theta$) the radial wind velocity $V = V(r)$ is decreased, and the density $\rho = \rho(r)$ is increased as compared with those outside the sector ($|\theta - \pi/2| > \Delta\theta$). A feature of the model is the strong discontinuity of values of V and ρ on lines $\theta = \pi/2 \pm \Delta\theta$. The form of the wave surface is sought after linearizing Equation (A21) by the method of harmonic analysis, using a weakly converging series. However, under the chosen initial and boundary conditions (the original surface of the front is a sphere, whose center coincides with the solar center; the homogeneity condition $\partial(\rho, V, D_n)/\partial\theta = 0$ inside and outside the HCS sector bounded by the discontinuities) the problem is solved rapidly and accurately by the 'ray' method. In this case, Equations (1) and (2) yield:

$$\begin{aligned} &\mathrm{d}r/\mathrm{d}t = V(r) + D_n(r)\,, \\ &\mathrm{d}\theta/\mathrm{d}t = \mathrm{d}\varphi/\mathrm{d}t = 0\,, \quad \mathbf{n} = \mathbf{e}_r\,. \end{aligned} \tag{A22}$$

It is easy to see that the trajectory of a small element of the shock front is a straight radial line. Assuming further, following the authors, $D_n/V = R = \text{constant}$, we find that the form of the front of a strong shock in the (r, θ)-plane exactly repeats the corresponding profile $V_r(\theta)$ in Figure 1 of the cited paper, which qualitatively coincides with the approximate solution obtained by the authors. The depth of the rectangular 'dimple' on the wave surface increases in accordance with the first Equation (A22). Our remark on this rather obvious result is as follows.

The technique used to determine the form of the front of a strong shock wave is applicable (as our used WKB method) only in the case of a weakly-inhomogeneous medium (because both methods reduce to seeking an accurate solution of the same Equation (A21). Therefore, the strong discontinuity of solar wind parameters on the lines $\theta = \pi/2 \pm \Delta\theta$ does not suggests the reality of the solution obtained, although it permits us to speak of a tendency for the wave energy to accumulate without limit in the neighbourhood of the HCS (at least, during some time). This means a strong pressure redistribution along the shock front, namely its growth in the HCS region. In addition to increasing the shock velocity in the neighbourhood of the HCS, this will also lead to a strong expansion of the sheet itself, with its subsequent slow compression. The increase in shock velocity, caused by a growth in its intensity in the immediate neighbourhood of the HCS (which is equivalent to the above-mentioned pressure redistribution behind the shock front) has been demonstrated just by our example of a smoothly-inhomogeneous model of the HCS.

Acknowledgements

We are grateful to Dr M. Dryer for stimulating discussions. We are also indebted to Mr V. G. Mikhalkovsky for his assistance in preparing the English version of the manuscript. The authors wish to thank the SCOSTEP project, SOLTIP (SOLar connection with Transient Interplanetary Processes), for partial support.

References

Barnes, A.: 1992, *Geophys. Res.* **97**(A8), 12 105.
Bazer, J. and Fleischman, O.: 1959, *Physics Fluids* **2**, 366.
Berstein, I. B.: 1971, *J. Plasma Physics* **5**, 303.
Bronshtein, I. N. and Semendyaev, K. A.: 1980, *Handbook on Mathematics*, Nauka, Moscow.
Blokhintsev, D. I.: 1981, *Acoustics of an Inhomogeneous Moving Medium*, Nauka, Moscow.
Burton, M. E., Siscoe, G. L., and Smith, E. J.: 1992, *Geophys. Res.* **97**(A8), 12 283.
Dryer, M., Wu, S. T., Wu, C. C., and Han, S. M.: 1992, *Proceedings of 26th ESLAB Symposium on Study of the Solar-Terrestrial System*, Killarney, Ireland (in press).
Eselevich, V. G., Uralova, S. V., and Uralov, A. M.: 1991, *Proceedings of the First SOLTIP Symposium*, Liblice, Czechoslovakia, Vol. 1, p. 110.
Gubkin, K. E.: 1961, 'Nonlinear Geometrical Acoustics and Its Applications', in *Nekotorye problemy matematiki i mekhaniki*, Novosibirsk.
Han, S. M., Wu, S. T., and Dryer, M.: 1988, *Computers and Fluids* **16**, 81.
Kerstenboim, Kh. S., Roslyakov, G. S., and Chudov, L. A.: 1974, *The Point Explosion*, Nauka, Moscow.
Korn, G. A. and Korn, T. P.: 1968, *Mathematical Handbook.*
Korobeinikov, V. P.: 1967, *Magnitnaya gidrodinamika*, No. 2, Zinatne, Riga, p. 25.
Kravtsov, Yu. A. and Orlov, Yu. I.: 1980, *Geometrical Optics of Inhomogeneous Media*, Nauka, Moscow.
Kulikovsky, A. G. and Lyubimov, G. A.: 1962, *Magnetic Hydrodynamics*, Moscow.
Uralova, S. V. and Uralov, A. M.: 1990, *Plasma Astrophysics*, European Space Agency Publ. ESA SP-311, Proceeings of joint Varenna–Abastumani–ESA–Nagoya–Potsdam Workshop, Telavi, Georgia, USSR, p. 99.
Uralov, A. M.: 1982, *Magnitnaya gidrodinamika*, No. 1, Zinatne, Riga, p. 45.
Watanabe, T.: 1989, *Adv. Space Res.* **9**(4), 99.
Wei, F. and Dryer, M.: 1991, *Solar Phys.* **132**, 373.
Weinberg, S.: 1962, *Phys. Rev.* **136**(6), 1899.
Yakovlev, O. I., Yefimov, A. I., and Rubtsov, S. N.: 1988, *Astron. Zh.* **65**(6), 1290.